

Collective effects in vortex movements in complex (dusty) plasmas

Mierk Schwabe,^{1,2,*} Sergey Zhdanov,² Christoph R ath,²
David B. Graves,¹ Hubertus M. Thomas,² and Gregor E. Morfill²

¹*Department of Chemical and Biomolecular Engineering,
University of California, Berkeley, CA 94720, USA*

²*Max Planck Institute for extraterrestrial Physics,
PO Box 1312, Giessenbachstr., 85741 Garching, Germany*

(Dated: September 20, 2018)

We study the onset and characteristics of vortices in complex (dusty) plasmas using two-dimensional simulations in a setup modeled after the PK-3 Plus laboratory. A small number of microparticles initially self-arranges in a monolayer around the void. As additional particles are introduced, an extended system of vortices develops due to a non-zero curl of the plasma forces. We demonstrate a shear-thinning effect in the vortices. Velocity structure functions and the energy and enstrophy spectra show that vortex flow turbulence is present that is in essence of the ‘‘classical’’ Kolmogorov type.

PACS numbers: 52.27.Lw, 52.65.-y, 52.35.Ra

Introduction—Complex plasmas consist of micrometer-sized particles embedded in a low temperature plasma. Experimenters can record the trajectories of the microparticles with digital cameras and study the microparticle behavior in detail. Complex plasmas are ideal model systems for nano fluids, phase transitions, transport processes, etc [1]. They display many collective effects. For instance, vortices in which the microparticles move in circles are common. They appear when gravity is compensated by thermophoresis [2–4] and in weightless systems [5–7] and can be induced externally, for instance by a laser [8, 9], by a probe [10, 11], or by gas flow [12–15]. Vortices can convoy nucleation [16] and lead to shear flow instabilities at their edges [17]. The origin of self-excited vortices in complex plasmas has long been a topic of discussion. They could be induced by the microparticle size dispersion [3, 18], charge gradients [19, 20], the void [21], or a non-zero curl of the forces that the plasma exerts on the microparticles [22, 23].

As we show in the following, vortices in complex plasmas are an ideal test-bed for studying the onset of turbulence and collective effects on the microcanonical level [2]. The description and dynamics of a turbulent complex plasma is an outstanding problem. Turbulence can be present in the background gas [14, 24] or plasma [25, 26] or induced by instabilities or waves in the dusty plasma itself [27–29]. In comparison with traditional experiments on turbulence (see, e.g., [30–32]), the particles that transmit the interaction can be visualized directly. Still many physical questions remain unanswered partly because the adequate simulations are lacking. Simulations help identify relevant experimental parameters and lead the way to designing related experiments.

Hybrid simulations are especially well suited to study self-excited vortices. In these simulations, the plasma is typically simulated as a fluid and coupled with a separate simulation of the microparticle dynamics. This allows

taking into account the forces that the plasma exerts on the microparticles and letting vortices develop naturally. Then, the reason for the self-excitation of vortices and the exact process of the onset of vortices can be determined.

Here, we present two-dimensional simulations of vortices in complex plasmas to investigate the onset of turbulence and collective effects. We model the discharge plasma and the cooperative dynamics of the microparticles embedded in it and demonstrate that the microparticle shear flow is relevant to that observed experimentally, and subjected to shear-thinning and turbulence.

Simulation particulars—We use the simulation setup described in [33], which is a two-dimensional model of the central plane of the PK-3 Plus chamber [34]. It consists of a hybrid fluid-analytical description of the plasma by Kawamura et al. [35], coupled to a molecular-dynamics (MD) simulation of the microparticle dynamics. The MD simulation is based on the Large-scale Atomic/Molecular Massively Parallel Simulator (LAMMPS) [36], modified to take into account the plasma forces. The microparticles interact via Yukawa pair potentials and are subject to random forces mimicking interactions with background atoms bumping into them. There is also a background friction force exerted by the neutral gas on the microparticles, the so-called Epstein drag force [37]. The ion flux and ambipolar electric field from the plasma simulation are used to calculate the ion drag and confinement forces acting on the microparticles. A naturally occurring non-vanishing curl of the sum of these forces leads to the generation of vortices.

For the simulations presented here, we use argon at a pressure of 10 Pa as buffer gas. The microparticles have a diameter of $3.4 \mu\text{m}$, a mass of $3.1 \times 10^{-14} \text{ kg}$, and a charge of $-3481e$. The friction constant with the background gas is $\gamma_{\text{EP}} = 37 \text{ s}^{-1}$. The electron temperature is 2.4 eV , the ion and neutral gas temperatures 300 K . The mean electron and ion number densities are $3.4 \times 10^{14} \text{ m}^{-3}$,

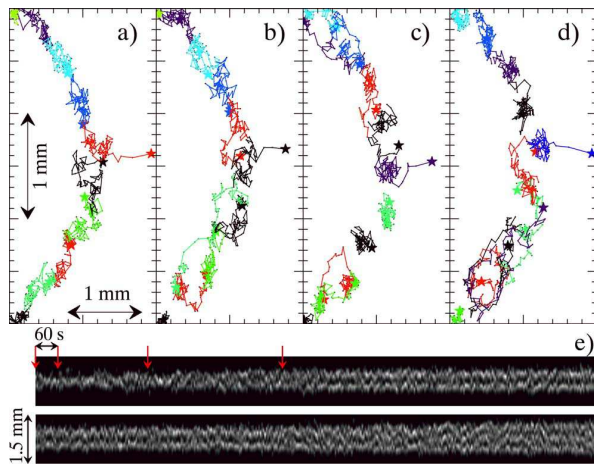


FIG. 1: (color online) (a-d) Trajectories that show the process of adding single particles to a monolayer. The trajectories of individual particles are distinguished by color. The start point of each trajectory is indicated by a star. e) Space-time plot (periodogram) that demonstrates the development of the width of the central part of the microparticle cloud with time. To make this picture, we added the pixel intensities of images showing the particle positions in the region $y = 9.5 - 10.5$ mm as a function of x position for frames corresponding to a total of 50 particle injections and plot the resulting graphs next to each other. In the periodogram, the vertical axis corresponds to x -position, and the horizontal axis to time. Injections occur every minute. The arrows indicate the injections a)-d).

with a maximum in the center of the simulation box (see [33]). We do not take into account the effect of the microparticles on the plasma. Unless otherwise mentioned, we used 7100 particles in the simulation runs presented here. The areal density of the cloud is $1.4 \times 10^7 \text{ m}^{-2}$.

Onset of vortices—We mimic the experimental injection process by placing microparticles near the sheath edge. They are then pushed into the plasma by the ambipolar electric field. Inside the plasma bulk, the ion drag force drives the microparticles around the void, where they arrange in a monolayer along the equilibrium line where the counteracting ion drag and ambipolar electric force are balanced. Figure 1 shows trajectories of particles inside this monolayer as progressively more particles are added. A single particle added to the monolayer rapidly finds a place inside (Fig. 1(a)). The next added particle is also incorporated into the monolayer, but the propagation of forces along the monolayer leads to a particle further down (shown in light green) being ejected from the layer. The ejected particle hops along the inside of the monolayer (Fig. 1(b)). The next particles that are injected disturb the layer, causing transverse displacement of other particles, but no vortices appear yet (Fig. 1(c)). Two layers of particles form, and vortex motion ensues only after the 12th particle injection (Fig. 1(d)). The space-time plot (periodogram) (Fig. 1(e)) demonstrates the growth of the cloud width with addi-

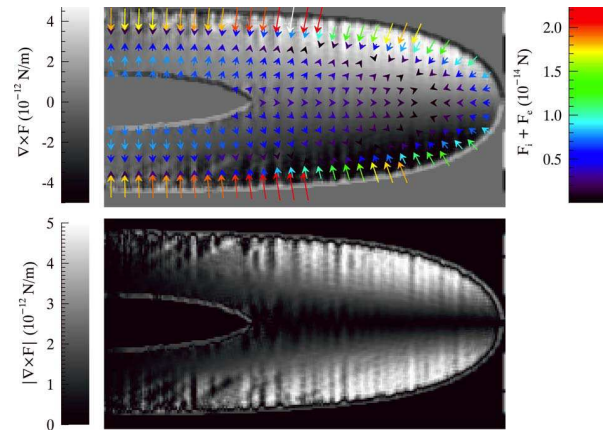


FIG. 2: (color online) (top) The sum of the ion drag F_i and electric force F_e acting on the particles (vectors, color online, right color map) overlaid a map of the curl of the force field (greyscale, left color map). The equilibrium line is clearly visible in the vector field. The edge of the cloud in the curl map is enhanced, which is an artefact of the way curl \mathbf{F} was calculated. (bottom) Map of the absolute value of the curl of the force field. Both curl maps uses a threshold of $\pm 5 \times 10^{-12} \text{ N/m}$ to enhance the contrast.

tional injections of single particles. An additional particle is injected every 60 s.

Figure 2 shows the vector plot of the combined plasma forces acting on the particles, the ion drag force F_i and the ambipolar electric force F_e . There is a single line around the void at which the sum of these two forces vanishes. This equilibrium line is visible in Fig. 2 as the line to which the vectors point. On the outside of the equilibrium line, the confining ambipolar electric force dominates, whereas on the inside of the equilibrium line, the ion drag force dominates, keeping the central 'void' particle-free. The cause of the finite width of the microparticle cloud is the mutual interparticle repulsion.

The gray-scaled background of Fig. 2 maps the non-zero component of the curl of the plasma force field, $\nabla \times (\mathbf{F}_i + \mathbf{F}_e)$ [42]. The magnitude of the curl of the vector field is largest near the edges of the microparticle cloud, on the outside of the equilibrium line, whereas it nearly vanishes on the inside of the equilibrium line and in the mid-plane of the simulation box. This qualitatively confirms the basic result of Akdim and Goedheer [22]: The vortices can be caused by a non-vanishing curl of the plasma force (see also [43]).

Fully developed system of vortices—Once several layers of microparticles are present, the vortices are fully developed. Figure 3 visualizes the movement of microparticles inside a cloud with two vortices. The particles move towards the simulation box center along the outside of the cloud and back towards the cloud edge in the central plane, as in the experiments in the PK-3 Plus laboratory on board the International Space Station [44].

The particles move fastest at the edge of the vortices,

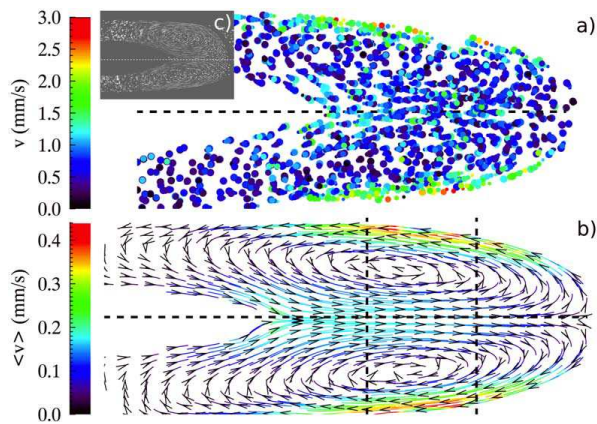


FIG. 3: (color online) Simulated (a,b) and experimental vortices (c). The horizontal dashed lines mark the chamber midplane/simulation box center. The field of view is (a,b) $23 \times 10 \text{ mm}^2$ and (c) $30 \times 20 \text{ mm}^2$. a) Positions of 1/10 of all particles in the simulation. The dots indicate four particle positions 0.2s apart for each particle and grow with time. The color of the dots indicates the total particle velocity, which is shown with a threshold of 3 mm/s. b) Streamlines and arrows indicate the mean velocity field of the simulated vortices. The mean was calculated by averaging over at least five particles for each position. The vertical dashed lines indicate the position of the sliding window used for Fig. 5. c) Overlay of 60 pictures (30s) taken with the PK-3 Plus laboratory, courtesy of the PK-3 Plus team [34]. The images are mirrored horizontally to correspond to the simulation.

where the rotational energy is concentrated, see Fig. 4 showing the enstrophy density of system. We calculate the enstrophy density following [17]: Firstly, we determine the 16 closest neighbors of every particle i and find the vectors to their positions $\mathbf{r}_{ij} = \mathbf{r}_j - \mathbf{r}_i$ and the relative velocities $\mathbf{v}_{ij} = \mathbf{v}_j - \mathbf{v}_i$. The vorticity ω_i is a function of the projections c_{ij} of the relative velocity onto the vectors orthogonal to \mathbf{r}_{ij} :

$$\omega_i = \mathbf{e}_z \cdot (\mathbf{curl} \mathbf{v})_i = \frac{1}{nn} \sum_{j=1}^{nn} c_{ij}, \quad (1)$$

where $nn = 16$ is the number of neighbors used in the calculation, $\mathbf{e}_z = \mathbf{e}_x \times \mathbf{e}_y$ is the unit vector in direction perpendicular to the plane of the simulation, and $c_{ij} = (\mathbf{e}_z \times \mathbf{r}_{ij}) \cdot \mathbf{v}_{ij} / r_{ij}^2$. Finally, we calculate the enstrophy density Ω_{kl} in every grid cell (k,l) from the average squared vorticity

$$\Omega_{kl} = \left(\frac{1}{n} \sum_{i=0}^n \omega_i \right)^2, \quad (2)$$

where n is the number of particles in the cell.

Figure 4 shows that the enstrophy density is concentrated at the edges of the microparticle cloud, where the microparticles move the fastest. As there are considerable velocity differences across the cloud, we shall next see whether the vortices produce any shear stress.

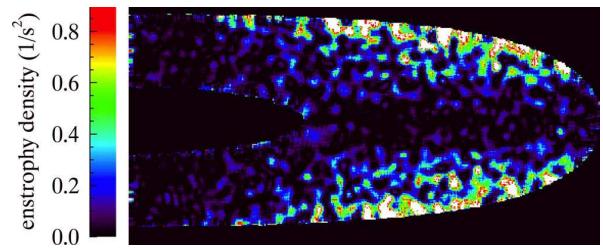


FIG. 4: (color online) Enstrophy density Ω of the vortices. Field of view: $23 \times 12 \text{ mm}^2$.

Shear thinning—We follow [38] to calculate the shear stress σ_{xy} , i.e., the off-diagonal elements of the pressure tensor, that is build up from the contributions of each particle's neighbors, neglecting the kinetic component. For a two-dimensional system in polar coordinates, σ_{xy} is given by

$$\sigma_{xy} = -\frac{1}{2}n^2 \int_0^{r_{max}} dr r^2 \frac{dV}{dr} \int_0^{2\pi} d\phi \cos \phi \sin \phi g(r, \phi), \quad (3)$$

where n is the number density of the microparticles, V is the Yukawa potential, and $g(r, \phi)$ is the radial pair distribution function. The insets (a) and (b) in Fig. 5 show the pair correlation functions at the upper and lower edges of the cloud. As in [38], the elliptical distortion of $g(r, \phi)$ shows strong shear stress.

The main part of Fig. 5 shows the shear rate $\gamma = (\partial v_x / \partial y) + (\partial v_y / \partial x)$, calculated from the velocity maps, and the shear stress σ_{xy} as a function of height above the lower sheath edge in a sliding window of size $5 \times 2 \text{ mm}^2$ at a horizontal distance of 12 mm from the plasma center (see Fig. 3). The vertical center of the simulation box is at a height of 10 mm. Both the shear rate and the shear stress vanish in the middle, where all particles are moving

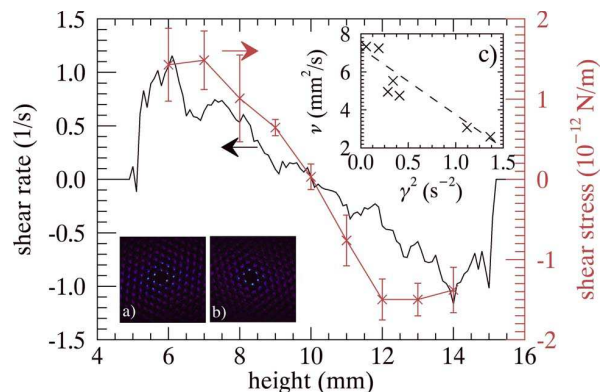


FIG. 5: (color online) Shear rate and shear stress as a function of height above the lower sheath edge. Insets: Radial pair correlation functions at the lower (a) and upper (b) edges of the cloud, c) viscosity ν as a function of squared shear stress γ^2 , demonstrating shear thinning. The dashed line is a guide to the eye.

towards the edge of the cloud. Their absolute values are largest close to the area where the opposite fluxes induced by the vortices meet, as expected. Numerically, the values are close to those found in experiments by Nosenko et al. [38], in which laser-induced motion of microparticles is studied. We also observe shear-thinning, as can be seen in Fig. 5(c) [45]: The viscosity $\nu = \sigma_{xy}/(\rho\gamma)$, with ρ being the areal mass density, decreases as a function of squared shear stress.

Flow velocity—The parameters of the simulated vortex flow fit real experiments performed with complex plasmas. For instance, using a mean viscosity of $\nu = 5 \text{ mm}^2/\text{s}$, a flow velocity of $v = 2 \text{ mm/s}$ and a typical size of the vortices of $L = 10 \text{ mm}$ (see Figs. 3,5), we obtain a Reynolds number $\mathcal{R} = vL/\nu \sim 4$, which is well in-line with observations [2, 17]. At such a low value, e.g., water flow is typically laminar. Nevertheless, we do find evidence that turbulence is present in the system of vortices, as we shall see next.

Turbulence—The origin of the turbulent pulsations in our simulations is twofold. It is the external normally-distributed random forces and the mutual interparticle interactions leading to randomization as well. Speaking about turbulence, first of all it is necessary to scale the fluctuations. Using the average viscosity $\nu = 5 \text{ mm}^2/\text{s}$ and the mean enstrophy density of $\Omega = 0.4 \text{ s}^{-2}$ obtained in simulations, we get an energy dissipation rate per unit mass [39] of the order of $\epsilon = 2\nu\Omega = 4 \text{ mm}^2/\text{s}^3$. This results in a Kolmogorov length scale of $L_K = (\nu^3/\epsilon)^{1/4} = 2.4 \text{ mm}$, which is an intermediate scale between the size of the simulation box ($20 \times 45 \text{ mm}^2$) and the interparticle distance (0.15 mm).

Traditionally, the scaling of vortices is studied by computing structure functions. The longitudinal structure functions of order p , $S_p(r)$, are given by

$$S_p(r) = \langle (\Delta u_r)^p \rangle = \langle [u(x+r) - u(x)]^p \rangle, \quad (4)$$

where $u(x)$ is the velocity component parallel to the relative displacement r . We use the absolute value of the velocity difference in the calculations, as this is more numerically stable and does not significantly change the results [30]. For fully developed turbulence, the structure functions show a power law scaling [39]

$$S_p \propto r^{\zeta_p}. \quad (5)$$

Kolmogorov [40] predicted the exponents to be given by $\zeta_p = p/3$. Figure 6 shows the horizontal velocity structure functions measured in the region to the right of the void, where the particles are flowing mainly in horizontal direction. As recommended by Lewis and Swinney [30], we use extended self-similarity [41], i.e., we plot S_p vs. S_3 on a log-log plot and use the fact that $\zeta_3 = 1$ according to Kolmogorov's theory. The slopes of the plots are then given by $\zeta_p/\zeta_3 = \zeta_p$. Figure 6 shows that the slopes

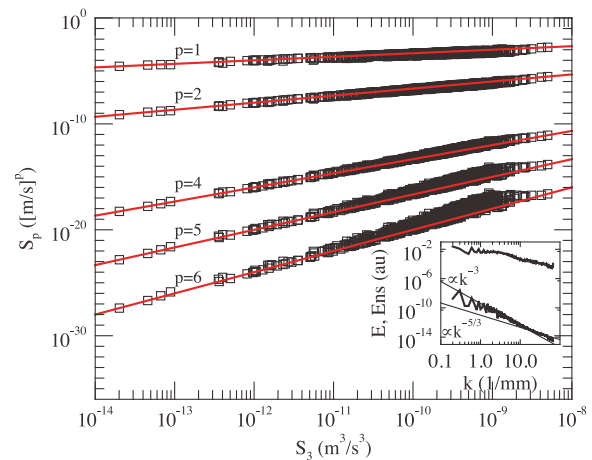


FIG. 6: (color online) Squares: First ($p=1$) through sixth ($p=6$) order longitudinal velocity structure functions S_p as a function of the third order structure function S_3 . The lines are those predicted by classical Kolmogorov theory $S_p \propto r^{\zeta_p}$, with $\zeta_p = p/3$. Inset: Energy (bottom) and Enstrophy density spectrum (top). The slopes of the lines overplotted on the energy spectrum are -3 and -5/3.

are very close to those predicted by Kolmogorov (as the overplotted solid lines in the figure indicate).

The inset in Fig. 6 shows the energy and enstrophy density spectra. The energy spectrum is calculated from the sum of the squares of the Fourier transformed velocity maps (see Fig. 3), the enstrophy spectrum from the enstrophy map (see Fig. 4). The two lines that are overplotted on the energy spectrum have the slopes -3 and -5/3, as expected: The $\propto k^{-5/3}$ dependence is typical inside the inertial range, and the cross-over to $\propto k^{-3}$ is due to friction [39].

Summary—To conclude, we numerically studied two-dimensional vortices in a complex plasma. We showed how these vortices develop from a monolayer around the void, and that a non-zero curl of the combined ion drag and electric forces causes the vortex movement of the microparticles. We then investigated the properties of fully developed system of vortices, for instance the flow field and shear stress. In particular, we showed that turbulence is present in the flow induced by the vortices and demonstrated that the velocity structure functions scale very close to the predictions by Kolmogorov theory. These results show that it should be possible to use common experimental situations like vortices in complex plasmas to study turbulence on the level of individual particles.

We acknowledge support by a Marie Curie International Outgoing Fellowship within the 7th European Community Framework Programme, from the European Research Council under the European Unions Seventh Framework Programme (FP7/2007- 2013)/ERC Grant Agreement No. 267499, and by the US Department of

Energy, Office of Fusion Science Plasma Science Center. The corresponding experiments on the International Space Station were funded by DLR/BMWi under the contract numbers FKZs 50 WM 0203 and 50 WM 1203.

* mierk@berkeley.edu

- [1] G. E. Morfill and A. V. Ivlev, *Rev. Mod. Phys.* **81**, 1353 (2009).
- [2] G. E. Morfill, M. Rubin-Zuzic, H. Rothermel, A. V. Ivlev, B. A. Klumov, H. M. Thomas, U. Konopka, and V. Steinberg, *Phys. Rev. Lett.* **92**, 175004 (2004).
- [3] M. Rubin-Zuzic, H. Thomas, S. Zhdanov, and G. E. Morfill, *New J. Phys.* **9**, 39 (2007).
- [4] M. Schwabe, M. Rubin-Zuzic, S. Zhdanov, A. V. Ivlev, H. M. Thomas, and G. E. Morfill, *Phys. Rev. Lett.* **102**, 255005 (2009).
- [5] G. E. Morfill, H. M. Thomas, U. Konopka, H. Rothermel, M. Zuzic, A. Ivlev, and J. Goree, *Phys. Rev. Lett.* **83**, 1598 (1999).
- [6] V. E. Fortov, O. S. Vaulina, O. F. Petrov, V. I. Molotkov, A. V. Chernyshev, A. M. Lipaev, G. Morfill, H. Thomas, et al., *JETP* **96**, 704 (2003).
- [7] A. P. Nefedov, G. E. Morfill, V. E. Fortov, H. M. Thomas, H. Rothermel, T. Hagl, A. V. Ivlev, M. Zuzic, et al., *New J. Phys.* **5**, 33 (2003).
- [8] M. Klindworth, A. Melzer, A. Piel, and V. A. Schweigert, *Phys. Rev. B* **61**, 8404 (2000).
- [9] T. Miksch and A. Melzer, *Phys. Rev. E* **75**, 016404 (2007).
- [10] D. A. Law, W. H. Steel, B. M. Annaratone, and J. E. Allen, *Phys. Rev. Lett.* **80**, 4189 (1998).
- [11] G. Uchida, S. Iizuka, T. Kamimura, and N. Sato, *Phys. Plasmas* **16**, 053707 (2009).
- [12] V. I. Vladimirov, L. V. Deputatova, A. P. Nefedov, V. E. Fortov, V. A. Rykov, and A. V. Khudyakov, *J. Exp. Theo. Phys.* **93**, 313 (2001).
- [13] S. Mitic, R. Sütterlin, A. V. Ivlev, H. Höfner, M. H. Thoma, S. Zhdanov, and G. E. Morfill, *Phys. Rev. Lett.* **101**, 235001 (2008).
- [14] M. Schwabe, L.-J. Hou, S. Zhdanov, A. V. Ivlev, H. M. Thomas, and G. E. Morfill, *New J. Phys.* **13**, 083034 (2011).
- [15] M. A. Fink, S. K. Zhdanov, M. Schwabe, M. H. Thoma, H. Höfner, H. M. Thomas, and G. E. Morfill, *EPL* **102**, 45001 (2013).
- [16] V. Nosenko, S. Zhdanov, and G. Morfill, *Phys. Rev. Lett.* **99**, 025002 (2007).
- [17] R. Heidemann, S. Zhdanov, K. R. Sütterlin, H. M. Thomas, and G. E. Morfill, *EPL* **96**, 15001 (2011).
- [18] T. Yokota and K. Honda, *J. Quant. Spectrosc. Radiat. Transfer* **56**, 761 (1996).
- [19] O. S. Vaulina, A. P. Nefedov, O. F. Petrov, and V. E. Fortov, *J. Exp. Theo. Phys.* **91**, 1147 (2000).
- [20] O. S. Vaulina, A. A. Samarian, O. F. Petrov, B. W. James, and V. E. Fortov, *New J. Phys.* **5**, 82 (2003).
- [21] A. A. Mamun and P. K. Shukla, *Phys. Plasmas* **11**, 1757 (2004).
- [22] M. R. Akdim and W. J. Goedheer, *Phys. Rev. E* **67**, 056405 (2003).
- [23] W. J. Goedheer and M. R. Akdim, *Phys. Rev. E* **68**, 045401(R) (2003).
- [24] S. Robertson and Z. Sternovsky, *IEEE Trans. Plas. Sci.* **35**, 314 (2007).
- [25] T. Klinger, C. Schröder, D. Block, F. Greiner, A. Piel, G. Bonhomme, and V. Naulin, *Phys. Plasmas* **8**, 1961 (2001).
- [26] S. Benkadda and V. N. Tsytovich, *Plasmas Phys. Rep.* **28**, 395 (2002).
- [27] P. K. Shukla, R. Bharuthram, and R. Schlickeiser, *Phys. Plasmas* **11**, 1732 (2004).
- [28] J. Pramanik, B. Veerasha, G. Prasad, and P. Kaw, *Phys. Lett. A* **312**, 84 (2003).
- [29] Y.-Y. Tsai, M.-C. Chang, and L. I, *Phys. Rev. E* **86**, 045402 (2012).
- [30] G. S. Lewis and H. L. Swinney, *Phys. Rev. E* **59**, 5457 (1999).
- [31] A. Arnèodo, R. Benzi, J. Berg, L. Biferale, E. Bodenschatz, A. Busse, E. Calzavarini, B. Castaing, et al., *Phys. Rev. Lett.* **100**, 254504 (2008).
- [32] R. Monchaux, *New J. Phys.* **14**, 095013 (2012).
- [33] M. Schwabe and D. B. Graves, *Phys. Rev. E* **88**, 023101 (2013).
- [34] H. M. Thomas, G. E. Morfill, V. E. Fortov, A. V. Ivlev, V. I. Molotkov, A. M. Lipaev, T. Hagl, H. Rothermel, et al., *New J. Phys.* **10**, 033036 (2008).
- [35] E. Kawamura, D. B. Graves, and M. A. Lieberman, *Plasma Sourc. Sci. Techn.* **20**, 035009 (2011).
- [36] S. Plimpton, *J. Comp. Phys.* **117**, 1 (1995), URL <http://lammps.sandia.gov>.
- [37] P. Epstein, *Phys. Rev.* **23**, 710 (1924).
- [38] V. Nosenko, A. V. Ivlev, and G. E. Morfill, *Phys. Rev. E* **87**, 043115 (2013).
- [39] U. Frisch, *Turbulence : the legacy of A.N. Kolmogorov* (Cambridge University Press, 1995).
- [40] A. N. Kolmogorov, *C. R. Acad. Sci. URSS* **30**, 9 (1941).
- [41] R. Benzi, S. Ciliberto, R. Tripicciono, C. Baudet, F. Masaioli, and S. Succi, *Phys. Rev. E* **48**, R29 (1993).
- [42] The enhancement of the borders of the cloud is an artefact of the calculation (we only calculate the force for positions with microparticles – outside of the cloud, the total force is thus zero in our calculation. The algorithm to calculate the curl acts as an edge detection algorithm as the gradient is largest where the force falls to zero.)
- [43] As is easy to check, this also readily follows from a simplified rotation balance: $|\nabla \times \mathbf{v}| \sim (m\gamma_{\text{eff}})^{-1} |\nabla \times \mathbf{F}|$, where $\gamma_{\text{eff}} = \gamma_{\text{Ep}} + \nu k_{\text{eff}}^2$ with $k_{\text{eff}} \sim 2\pi/L_K$.
- [44] Note that in experiments, more complicated situations exist as well, for instance a reversal of the direction of rotation or a system with several vortices, which we have not observed in simulations so far.
- [45] Values with $\gamma^2 < 0.05 \text{ s}^{-2}$ were omitted in the plot, as the viscosity cannot be calculated by the above formula for γ^2 that are too small [38].